ARTICLE

Itinerant Flat-Band Magnetism in Hydrogenated Carbon Nanotubes

Xiaoping Yang[†,*] and Gang Wu[‡,*]

[†]Max-Planck-Institut für Festkörperforschung, Heisenbergstrasse 1, D-70569, Stuttgart, Germany, and [‡]Institute of High Performance Computing, 1 Fusionopolis Way, #16-16 Connexis, Singapore 138632, Singapore

ABSTRACT We investigate the electronic and magnetic properties of hydrogenated carbon nanotubes using *ab initio* spin-polarized calculations within both the local density approximation (LDA) and the generalized gradient approximation (GGA). We find that the combination of charge transfer and carbon network distortion makes the spin-polarized flat-band appear in the tube's energy gap. Various spin-dependent ground state properties are predicted with the changes of the radii, the chiralities of the tubes, and the concentration of hydrogen. It is found that strain or external electric field can effectively modulate the flat-band spin-splitting and even induce an insulator—metal transition.

KEYWORDS: hydrogenated carbon nanotube · density functional calculation · spin-polarized electronic structure · strain effect · electric field effect

Much attention has long been devoted to finding macroscopic magnetic ordering phenomena in organic materials. Experimentally, ferromagnetism has been discovered in pure carbon systems, such as carbon foam, graphite, oxidized C_{60}, and polymerized rhombohedral C_{60},[1−8] which has stimulated renewed interests in their fundamental importance and potential applications in high-technology (*e.g.*, spintronics). Much theoretical work has been done to study magnetism in nanographites,[9−17] C_{60} polymers,[18] and all-carbon nanostructures.[19−22] However, the microscopic origin of ferromagnetism remains controversial.

The recent proton irradiation experiments in graphite[2−5] have shown the importance of hydrogen in inducing the magnetization instead of magnetic impurities. Disorder induced by He^+ ion irradiation does not produce such a large magnetic moment as obtained with protons.[23] Theoretically, the possible magnetism arising from the adsorption of hydrogen atom on graphite has been studied.[16,17] It can be easily speculated that hydrogen can trigger the sp^2-sp^3 transformation, promoting the magnetic ordering in other carbon structures, especially carbon nanotubes with a surface of positive curvature.

Herein, we focus on the electronic and magnetic properties of single-walled carbon nanotubes (SWNTs) with hydrogen atoms adsorbed on their surfaces. Our results show that hydrogenated carbon nanotubes are on the verge of magnetism instability, and the combination of charge transfer and carbon network distortion drives flat-band ferromagnetism. To our knowledge, this is the first comprehensive *ab initio* study on the physical origin of flat-band ferromagnetism in the real carbon nanotube materials. Moreover, the applied strain and external electric field are found to have a strong influence on the flat-band spin-splitting, resulting in the variation of spin-relevant physical properties.

RESULTS AND DISCUSSION

Instead of the simple sp^2 bonds in graphite, the bonds in carbon nanotubes are of sp^2-sp^3 character due to the tube's curvature effect, making the hybridization of σ, σ^*, π, and π^* orbitals quite larger, especially for small-diameter tubes. Thus the magnetic properties of hydrogenated SWNTs are more complicated than that of hydrogenated graphite, with a large dependence on the radii, the chiralities, and hydrogen concentration. Here, two types of linear hydrogen concentration A and B are shown in Figure 1. There is one hydrogen atom per tube period in the higher concentration A and one hydrogen atom per every two tube periods in the lower concentration B. The higher H concentration leads to a larger structure deformation, as can be seen in Figure 1. Stable C−H bond length is 1.1 Å, typical of covalent bonding (*cf.* 1.09 Å in methane). Recently, the cooperative alignment of the absorbed atoms has been

*Address correspondence to xp.yang@fkf.mpg.de, wugaxp@gmail.com.

Received for review January 20, 2009 and accepted June 17, 2009.

Published online June 23, 2009. 10.1021/nn900379y CCC: $40.75

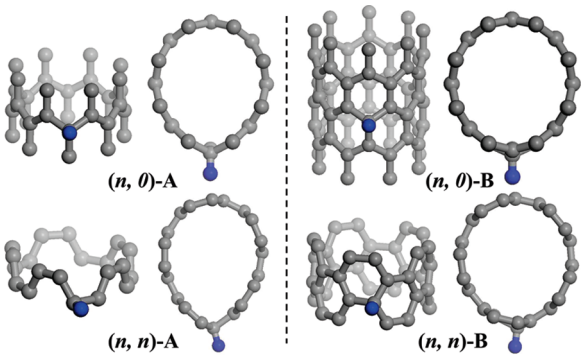

Figure 1. Schematic geometrical structures of hydrogenated zigzag (top panels) and armchair (bottom panels) tubes in the higher hydrogen concentration A with one hydrogen per tube period, or the lower hydrogen concentration B with one hydrogen per every two tube periods. Blue (gray) balls represent the hydrogen (carbon) atoms.

observed in graphene experimentally.[24] In the case of carbon nanotubes, the absorption of hydrogen on the tube wall is easier than that on graphene due to the curvature effect.[25] Moreover, the adatoms' cooperative alignment can be enhanced by high curvature regions of nanotube[25] that can result from pressure,[26] compression transverse to its axis,[25,27] or tube−substrate interaction.[28]

Now, let us study electronic structures of hydrogenated SWNTs, taking the zigzag (8,0), (9,0), armchair (5,5) and (10,10) tubes as examples. Figure 2 presents their ground state band structures obtained by using spin-polarized LDA (left panels) and GGA (PBE exchange correlation functional) (right panels). In spin-unpolarized LDA and GGA paramagnetic (PM) band structures (not shown here completely), a common feature is that a hydrogen atom induces a half-filled flat-band in the tube's energy gap around ε_F due to the odd electrons in compounds, as seen in the LDA PM ground state band structure of (5,5)-B in Figure 2. Apparently, flat-band causes an extremely high density of states around ε_F, and if the Coulomb interaction between itinerant electrons in the band is introduced, magnetic instability would occur. It has been shown that flat-band leads to ferromagnetism for certain models.[29] In hydrogenated SWNTs, the spin−spin interaction plays a similar role as the Coulomb one and lifts the spin degeneracy of the flat band. As a result, the flat-band's spin-splitting magnitude and the energy position relative to ε_F determine the ground state properties of system. As we can see in the right panels of Figure 2, the spin-splitting magnitude has increased after introducing the generalized gradient correction in the exchange correlation functional, compared to the LDA without correction (left panels), which makes the ferromagnetic (FM) state become more favorable in energy. The adsorption of the hydrogen atom is found to hardly affect the gaps of zigzag (8,0) and (9,0) tubes,[30,31] while a large tube's energy gap is opened in the metallic armchair (5,5) and (10,10) tubes. In the LDA results, (8,0)-A,B, (5,5)-A, and (10,10)-A exhibit FM semiconducting characteristics, whereas (9,0)-A,B and (10,10)-B are FM metals. (5,5)-B has a PM metallic ground state under LDA. However, the enhanced spin-splitting in GGA makes (9,0)-A,B and (10,10)-B present a FM semiconducting behavior, not metallic one under LDA. Furthermore, a FM metallic state is produced for (5,5)-B, not the PM metallic one obtained by LDA.

In order to investigate the physical origin of flat-band ferromagnetism, we plot the spin-up density of the full-occupied GGA flat-band of (9,0)-B (black band, see Figure 2) in Figure 3. A sp^3-like hybridization is induced on the carbon atom attached to the hydrogen atom, leading to whole carbon network distortion, accompanied by charge transfer from hydrogen to the bonded carbon atom (0.352 and 0.334 electron for LDA and GGA (PBE), respectively). Magnetism is strong itinerant in both circumferential and tube axial directions, arising from the hybridization of H s orbital with tube π

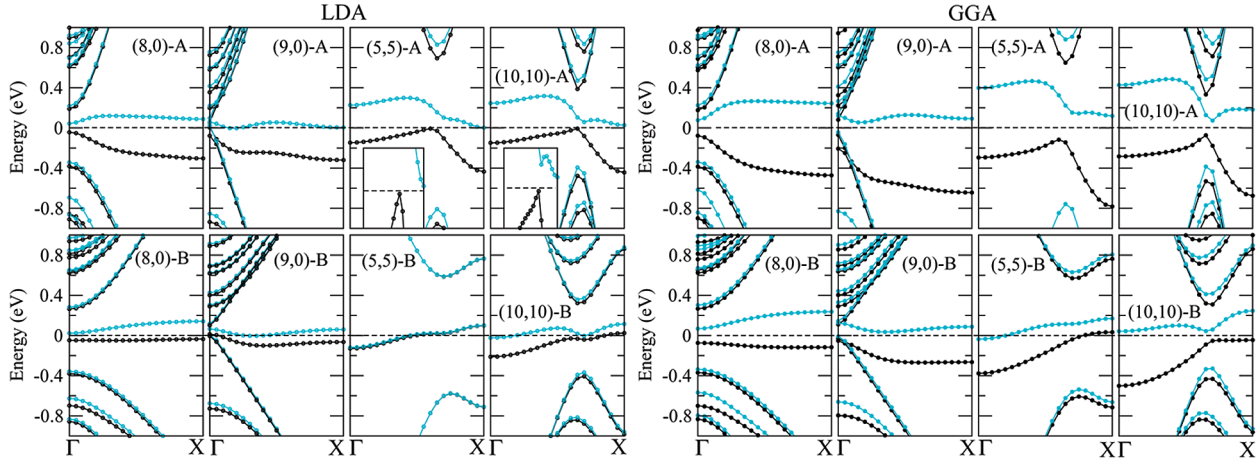

Figure 2. Spin-polarized LDA (left panels) and GGA (right panels) ground state band structures of hydrogenated zigzag (8,0) and (9,0), and armchair (5,5) and (10,10) tubes in the two different systems A (top panels) and B (bottom panels). Insets show the band structures around ε_F in an enlarged energy scale. The Fermi level is set at zero. Spin-up and spin-down channels are represented by black and cyan, respectively.

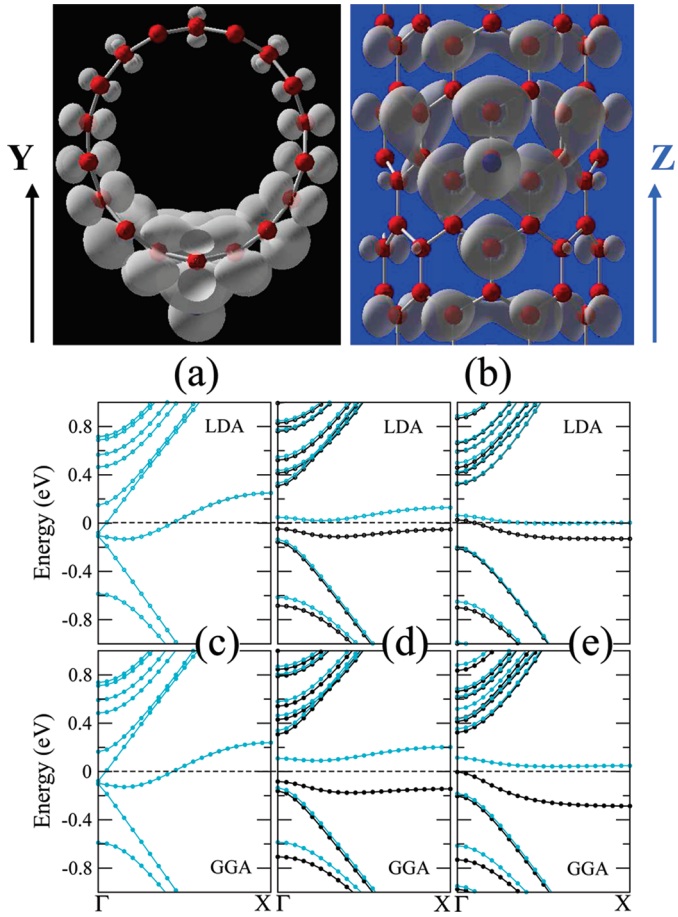

Figure 3. The 0.003 Å^{-3} magnetization density isosurfaces for the full-occupied spin-up GGA flat-band in (9,0)-B: (a) top view and (b) front view. Spin-polarized LDA and GGA ground state band structures for (9,0)-B: (c) with only the location of hydrogen atom relaxed, (d) under the 4% axial stretch strain, (e) under the 4% axial compression strain.

orbitals. Magnetic moments per unit cell are 0.63 and 0.96 μ_B in LDA and GGA, respectively.

Obviously, this s−π hybridization is relevant to structure distortion and affects the flat-band spin-splitting magnitude. To get such an insight, we carried out both LDA and GGA calculations on the undistorted (9,0)-B structure with only the location of the hydrogen atom relaxed. Charge transfer still exists, and the band structures plotted in Figure 3c clearly show a disappearance of the flat-band spin-splitting and also magnetism. Weak magnetic moment 0.2 μ_B per unit cell appears even if on-site Coulomb repulsion, U = 3.0 eV,[32] is considered in the LDA+U calculation. These results indicate that only charge transfer is not sufficient to induce a large magnetic moment; therefore, structure distortion is indispensable. As a result, we can anticipate that the applied strain could tune the physical properties of hydrogenated SWNTs by affecting the spin-splitting of flat-band. We applied a 4% stretch or compression strain along the tube axis, then the atomic positions were optimized again. Corresponding ground state electronic structures are given in Figure 3d,e. As expected, strain does have an important effect on the magnetic ground state properties. The 4% axial stretch strain causes the length of C−C bonds, beneath the H atom, to further stretch and deviate from the regular value of 1.42 Å, which enlarges the energy gap, as shown in Figure 3d. Even a metal−insulator transition is found in LDA band structure, accompanied by an increase in the magnetic moment to 0.96 μ_B (normally 0.63 μ_B). Under 4% axial compression strain, the compound presents the metallic or semiconducting characteristics similar to those without strain in both LDA and GGA, but the magnetic moment in LDA is reduced to 0.53 μ_B. Under both axial strains, the transferred charge remains 0.35−0.36 electrons in LDA and 0.33−0.34 electrons in GGA, proving that carbon network distortion plays a very important role in the flat-band spin-splitting. Of course, flat-band and magnetism would also disappear if we remove the hydrogen atom from the distorted SWNTs, indicating the necessity of hydrogen in inducing the ferromagnetic ordering, which is similar to the role of so-called "carbon radicals" in magnetic all-carbon structures.[12,13]

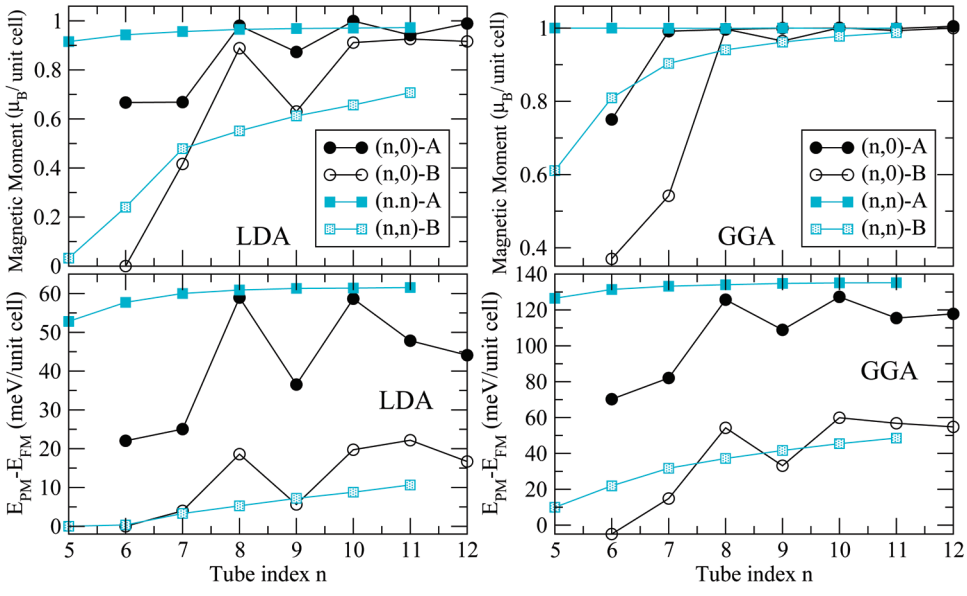

Figure 4. From the top down, the evolution of magnetic moment per unit cell and energy difference (E_{PM} − E_{FM}) per unit cell *vs* the tube index *n*. Left panels are from spin-polarized LDA, and right panels are from spin-polarized GGA (PBE).

Figure 4 summarizes structure information and ground state properties of hydrogenated zigzag (n,0) (n = 6−12) and armchair (n,n)

($n = 5-11$) tubes in both A and B cases (see Figure 1). Generally speaking, magnetic moment per unit cell has increased gradually with the change of tube index n (top panels) and approaches a saturation value in both LDA and GGA results. In the (n,0)-A case, the magnetic moment curve presents oscillation behavior (especially in LDA) that might be relevant to periodic change of the band gap in zigzag-type tubes. The higher concentration A-type compounds have a magnetic moment larger than that of the lower concentration B-type compounds, especially in smaller diameter tubes. In the bottom panels of Figure 4, the curves of energy difference ($E_{PM} - E_{FM}$) between FM and PM states per unit cell *versus* tube index n present a similar trend as found in the curves of magnetic moment *versus* n. Introducing of the generalized gradient correction enhances the spin-splitting, as discussed for Figure 2, which leads that the FM state becomes more favorable in GGA than in LDA, evidenced by the energy difference $E_{PM} - E_{FM}$. This reveals that magnetic properties of hydrogenated carbon nanotubes are affected by the structure characteristic of the SWNTs and the concentration of hydrogen.

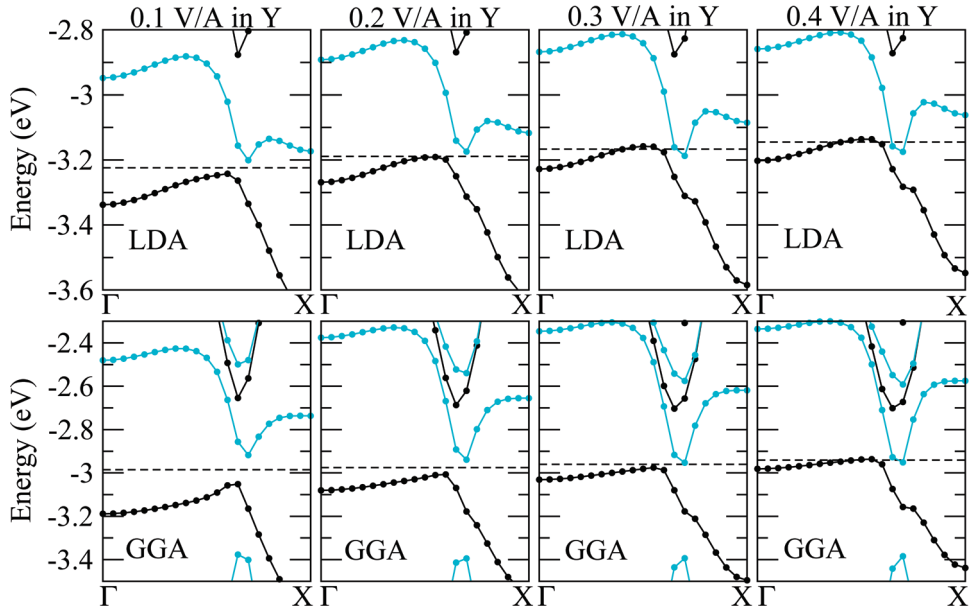

Figure 5. Spin-polarized LDA (top panels) and GGA (bottom panels) ground state band structures of hydrogenated armchair (10,10)-A with the applied electric fields in the modulus of 0.1−0.4 V/Å along the *Y* direction of cross section (see Figure 3a). The Fermi levels are marked in black dashed lines.

Finally, we also investigate the effect of transverse electric fields in the *Y* direction of cross section (see Figure 3a). Absorption of a H atom makes the SWNT become a polar organic compound. Here, the polar C−H bond is just along the *Y* direction. It can be anticipated that charge redistribution driven by an external electric field could occur, which would induce a subtle change of electronic structure. Both LDA and GGA simulations on (10,10)-A reveal the spin-dependent effect of applied external electric fields with a magnitude of 0.1−0.4 V/Å, illustrated in Figure 5. Compared with Figure 2, the applied field gradually decreases the gap between spin-up and spin-down flat-band at 0.1 and 0.2 V/Å, finally closes it, and directly drives an insulator−metal transition at 0.3 V/Å in LDA and 0.4 V/Å in GGA. This effect is different from the case of graphene nanoribbons,[9−11] where the band gap closure takes place only for one spin channel. The fantastic "beating" behavior of spin-polarized flat-band under the external electric field can be used for designing quantum switches.

CONCLUSIONS

We have demonstrated how the combined effect of charger transfer and carbon network distortion makes spin-polarized flat-band appear in the tube's energy gap, based on spin-polarized LDA and GGA (PBE) calculations, which is the origin of a variety of spin-relevant physical properties. Furthermore, hydrogenated SWNTs' ground state properties are found to depend largely on the radii, the chiralities of the SWNTs, and the concentration of hydrogen. Applied strain and transverse electric field can effectively tune the flat-band spin-splitting strength and even induce insulator−metal transition. Our results indicate that hydrogenated SWNTs are the promising candidates for the carbon-based nanometer ferromagnetism, spintronic devices, and even quantum switches. Also, the intrinsic ferromagnetism mechanism revealed in our paper can be applied to hydrogenated graphene and other carbon-based material with extended surface.

THEORETICAL METHODS AND MODELS

We carried out the numerical calculations using the Vienna *ab initio* Simulation Package (VASP)[33−36] within the framework of spin-polarized local density approximation (LDA) and generalized gradient approximation (GGA) (PBE exchange correlation functional).[37,38] The ion-electron interaction was modeled by the projector augmented wave (PAW) method[39,40] with a uniform energy cutoff of 400 eV. We used periodic boundary conditions and a supercell large enough to prohibit the electronic and the dipole−dipole interactions between neighboring tubes. The spacing between k points was 0.03 Å^{-1}: 1 × 1 × 8 k-point sampling in (n,0)-A, 1 × 1 × 4 in (n,0)-B, 1 × 1 × 14 in (n, n)-A, and 1

× 1 × 7 in (*n*, *n*)-B. The geometrical structures of hydrogenated SWNTs were optimized by employing the conjugate gradient technique, and in the final geometry, no force on the atoms exceeded 0.01 eV/Å.

Acknowledgment. We gratefully acknowledge O. K. Andersen for his encouragement and support, and Jinming Dong for useful discussion. X.Y. also thanks Shuiquan Deng, Jianwei Tong, and Joseph Law for a critical reading of the manuscript.

REFERENCES AND NOTES

1. Rode, A. V.; Gamaly, E. G.; Christy, A. G.; Fitz Gerald, J. G.; Hyde, S. T.; Elliman, R. G.; Luther-Davies, B.; Veinger, A. I.; Androulakis, J.; Giapintzakis, J. Unconventional Magnetism in All-Carbon Nanofoam. *Phys. Rev. B* **2004**, *70*, 054407–054415.
2. Esquinazi, P.; Setzer, A.; Höhne, R.; Semmelhack, C.; Kopelevich, Y.; Spemann, D.; Butz, T.; Kohlstrunk, B.; Lösche, M. Ferromagnetism in Oriented Graphite Samples. *Phys. Rev. B* **2002**, *66*, 024429–024438.
3. Esquinazi, P.; Spemann, D.; Höhne, R.; Setzer, A.; Han, K.-H.; Butz, T. Induced Magnetic Ordering by Proton Irradiation in Graphite. *Phys. Rev. Lett.* **2003**, *91*, 227201–227204.
4. Coey, J. M. D.; Venkatesan, M.; Fitzgerald, C. B.; Douvalis, A. P.; Sanders, I. S. Ferromagnetism of a Graphite Nodule from the Canyon Diablo Meteorite. *Nature* **2002**, *420*, 156–159.
5. Esquinazi, P.; Höhnea, R.; Hana, K. H.; Setzera, A.; Spemannb, D.; Butzb, T. Magnetic Carbon: Explicit Evidence of Ferromagnetism Induced by Proton Irradiation. *Carbon* **2004**, *42*, 1213–1218.
6. Murakami, Y.; Suematsu, H. Magnetism of C_{60} Induced by Photo-assisted Oxidation. *Pure Appl. Chem.* **1996**, *68*, 1463–1467.
7. Makarova, T. L.; Sundqvist, B.; Höhne, R.; Esquinazi, P.; Kopelevich, Y.; Scharff, P.; Davydov, V. A.; Kashevarova, L. S.; Rakhmanina, A. V. Magnetic Carbon. *Nature* **2001**, *413*, 716–718.
8. Wood, R. A.; Lewis, M. H.; Lees, M. R.; Bennington, S. M.; Cain, M. G.; Kitamura, N. Ferromagnetic Fullerene. *J. Phys.: Condens. Matter* **2002**, *14*, L385–L391.
9. Kusakabe, K.; Maruyama, M. Magnetic Nanographite. *Phys. Rev. B* **2003**, *67*, 092406–092409.
10. Son, Y.-W.; Cohen, M. L.; Louie, S. G. Half-Metallic Graphene Nanoribbons. *Nature* **2006**, *444*, 347–349.
11. Son, Y.-W.; Cohen, M. L.; Louie, S. G. Energy Gaps in Graphene Nanoribbons. *Phys. Rev. Lett.* **2006**, *97*, 216803–216806.
12. Fujita, M.; Wakabayashi, K.; Nakada, K.; Kusakabe, K. Peculiar Localized State at Zigzag Graphite Edge. *J. Phys. Soc. Jpn.* **1996**, *65*, 1920–1923.
13. Nakada, K.; Fujita, M.; Dresselhaus, G.; Dresselhaus, M. S. Edge State in Graphene Ribbons: Nanometer Size Effect and Edge Shape Dependence. *Phys. Rev. B* **1996**, *54*, 17954–17961.
14. Lehtinen, P. O.; Foster, A. S.; Ayuela, A.; Krasheninnikov, A.; Nordlund, K.; Nieminen, R. M. Magnetic Properties and Diffusion of Adatoms on a Graphene Sheet. *Phys. Rev. Lett.* **2003**, *91*, 017202–017205.
15. Ma, Y.; Lehtinen, P. O.; Foster, A. S.; Nieminen, R. M. Magnetic Properties of Vacancies in Graphene and Single-Walled Carbon Nanotubes. *New J. Phys.* **2004**, *6*, 68–82.
16. Lehtinen, P. O.; Foster, A. S.; Ma, Y.; Krasheninnikov, A. V.; Nieminen, R. M. Irradiation-Induced Magnetism in Graphite: A Density Functional Study. *Phys. Rev. Lett.* **2004**, *93*, 187202–187205.
17. Yazyev, O. V. Magnetism in Disordered Graphene and Irradiated Graphite. *Phys. Rev. Lett.* **2008**, *101*, 037203–037206.
18. Andriotis, A. N.; Menon, M.; Sheetz, R. M.; Chernozatonskii, L. Magnetic Properties of C_{60} Polymers. *Phys. Rev. Lett.* **2003**, *90*, 026801–026804.
19. Park, N.; Yoon, M.; Berber, S.; Ihm, J.; Osawa, E.; Tománek, D. Magnetism in All-Carbon Nanostructures with Negative Gaussian Curvature. *Phys. Rev. Lett.* **2003**, *91*, 237204–237207.
20. Zhang, Y.; Talapatra, S.; Kar, S.; Vajtai, R.; Nayak, S. K.; Ajayan, P. M. First-Principles Study of Defect-Induced Magnetism in Carbon. *Phys. Rev. Lett.* **2007**, *99*, 107201–107204.
21. Yang, X.; Dong, J. Ferromagnetism of an All-Carbon Composite Composed of a Carbon Nanowire Inside a Single-Walled Carbon Nanotube. *Appl. Phys. Lett.* **2005**, *86*, 163105–163107.
22. Pei, X.; Yang, X.; Dong, J. Effects of Different Hydrogen Distributions on the Magnetic Properties of Hydrogenated Single-Walled Carbon Nanotubes. *Phys. Rev. B* **2006**, *73*, 195417–195420.
23. Han, K.-H.; Spemann, D.; Esquinazi, P.; Höhne, R.; Riede, V.; Butz, T. Ferromagnetic Spots in Graphite Produced by Proton Irradiation. *Adv. Mater.* **2003**, *15*, 1719–1722.
24. Li, J.-L.; Kudin, K. N.; McAllister, M. J.; Prud'homme, R. K.; Aksay, I. A.; Car, R. Oxygen-Driven Unzipping of Graphitic Materials. *Phys. Rev. Lett.* **2006**, *96*, 176101–176104.
25. Gülseren, O.; Yildirim, T.; Ciraci, S. Tunable Adsorption on Carbon Nanotubes. *Phys. Rev. Lett.* **2001**, *87*, 116802–116805.
26. Chesnokov, S. A.; Nalimova, V. A.; Rinzler, A. G.; Smalley, R. E.; Fischer, J. E. Mechanical Energy Storage in Carbon Nanotube Springs. *Phys. Rev. Lett.* **1999**, *82*, 343–346.
27. Mazzoni, M. S. C.; Chacham, H. Bandgap Closure of a Flattened Semiconductor Carbon Nanotube: A First-Principles Study. *Appl. Phys. Lett.* **2000**, *76*, 1561–1563.
28. Hertel, T.; Walkup, R. E.; Avouris, P. Deformation of Carbon Nanotubes by Surface van der Waals Forces. *Phys. Rev. B* **1998**, *58*, 13870–13873.
29. Tasaki, H. From Nagaoka's Ferromagnetism to Flat-Band Ferromagnetism and Beyond—An Introduction to Ferromagnetism in the Hubbard Model. *Prog. Theor. Phys.* **1998**, *99*, 489–548.
30. Miyake, T.; Saito, S. Band-Gap Formation in (*n*,0) Single-Walled Carbon Nanotubes (n = 9,12,15,18): A First-Principles Study. *Phys. Rev. B* **2005**, *72*, 073404–073407.
31. Ouyang, M.; Huang, J.-L.; Cheung, C. L.; Lieber, C. M. Energy Gaps in "Metallic" Single-Walled Carbon Nanotubes. *Science* **2001**, *292*, 702–705.
32. Perfetto, E.; Cini, M.; Ugenti, S.; Castrucci, P.; Scarselli, M.; Crescenzi, M. D.; Rosei, F.; Khakani, M. A. E. Electronic Correlations in Graphite and Carbon Nanotubes from Auger Spectroscopy. *Phys. Rev. B* **2007**, *76*, 233408–233411.
33. Kresse, G.; Hafner, J. *Ab Initio* Molecular Dynamics for Liquid Metals. *Phys. Rev. B* **1993**, *47*, 558–561.
34. Kresse, G.; Hafner, J. *Ab Initio* Molecular-Dynamics Simulation of the Liquid-Metal-Amorphous-Semiconductor Transition in Germanium. *Phys. Rev. B* **1994**, *49*, 14251–14269.
35. Kresse, G.; Furthmüller, J. Efficient Iterative Schemes for *Ab Initio* Total-Energy Calculations Using a Plane-Wave Basis Set. *Phys. Rev. B* **1996**, *54*, 11169–11186.
36. Kresse, G.; Furthmüller, J. Efficiency of *Ab-Initio* Total Energy Calculations for Metals and Semiconductors Using a Plane-Wave Basis Set. *Phys. Rev. B* **1996**, *6*, 15–50.
37. Ceperley, D. M.; Alder, B. J. Ground State of the Electron Gas by a Stochastic Method. *Phys. Rev. Lett.* **1980**, *45*, 566–569.
38. Perdew, J. P.; Burke, K.; Ernzerhof, M. Generalized Gradient Approximation Made Simple. *Phys. Rev. Lett.* **1996**, *77*, 3865–3868.
39. Kresse, G.; Joubert, D. from Ultrasoft Pseudopotentials to the Projector Augmented-Wave Method. *Phys. Rev. B* **1999**, *59*, 1758–1775.
40. Blöchl, P. E. Projector Augmented-Wave Method. *Phys. Rev. B* **1994**, *50*, 17953–17979.